PRESSURE DISTRIBUTIONS AND OIL-FLOW PATTERNS FOR A SWEPT CIRCULATION-CONTROL WING

Earl R. Keener, Dwight T. Sanderfer, and Norman J. Wood*

Ames Research Center

SUMMARY

Pressure distributions and photographs of oil-flow patterns are presented for a circulation-control wing. The model was an aspect-ratio-four semispan wing mounted on the side wall of the NASA Ames 6- by 6-Foot Transonic Wind Tunnel. The airfoil was a 20%-thick ellipse, modified with circular leading and trailing edges of 4% radius, and had a 25.4-cm constant chord. This configuration does not represent a specific wing design, but is generic for research purposes. A full-span, tangential, rearward-blowing, circulation-control slot was incorporated ahead of the trailing edge on the upper surface. The wing was tested at Mach numbers from 0.3 to 0.75 at sweep angles of 0° and +45° with internal-to-external pressure ratios of 1.0 to 3.0. Lift and pitching-moment coefficients were obtained from measured pressure distributions at five span stations.

Oil-flow tests at 0° angle of attack show that the boundary layer separated just ahead of the slot. However, the flow attaches quickly with active jet blowing. The wing-surface flow at 45° sweep is nearly streamwise away from the leading edge. The wingtip flow is strongly entrained into the outer jet flow. The lower-surface boundary layer separates noticeably ahead of the Coanda-surface separation. The wingtip flow pattern is similar to that of the lee side of an ellipsoid at a 45° angle of attack. At 5° angle of attack, it is more difficult to attach the separated flow ahead of the slot with jet blowing at the lower speeds. At Mach 0.7 the separated flow cannot be attached ahead of the slot.

When the conventional corrections resulting from sweep angle are applied to the lift and moment of circulation-control sections, no additional corrections are necessary to account for changes in blowing efficiency. This is demonstrated herein for an aft sweep angle of 45°. An empirical technique for estimating the downwash distribution of a swept wing has been validated with the swept-wing data.

---

*Joint Institute for Aeronautics and Acoustics, Stanford University, Stanford, CA

NOMENCLATURE

AR	aspect ratio of semispan wing, b/2c
b/2	wing semispan, normal to plane of symmetry when swept
c	wing normal chord
c_ℓ	wing-section lift coefficient obtained from c_n and α
c_m	wing-section pitching-moment coefficient about c/2 obtained by numerical integration of pressures at each row of orifices
c_n	wing-section normal-force coefficient obtained by numerical integration of pressures at each row of orifices
C_p	pressure coefficient, $(p - p_\infty)/q_\infty$
C_μ	wing-section jet-momentum coefficient, $m_j V_j/q_\infty \, c \, l_j$
h/c	slot height/chord ratio
l_j	length of slot
M_∞	free-stream Mach number
m_j	jet mass flow computed from orifice-plate flow equations and measurements
PR	jet pressure ratio, plenum/tunnel static
q_∞	free-stream dynamic pressure
R_e	Reynolds number based on c
S/2	exposed wing area of semispan model
V_j	computed jet velocity assuming isentropic expansion from jet total pressure to free-stream static pressure
x	chordwise distance rearward of leading edge
y	spanwise distance outboard of wing root
α	angle of attack

Λ angle of sweep

η span station, 2y/b

Subscripts

j jet parameter

∞ free-stream conditions

N normal (free-stream) conditions

INTRODUCTION

There are several ways to control the aerodynamic circulation of wings and, thus, to control the amount of lift. One type of circulation control that is currently under investigation is tangential blowing out of a slot located ahead of a rounded trailing edge. For reasons not entirely understood, the flow adheres to the trailing-edge surface, which is known as the Coanda effect. The deflected flow increases the lift of a wing section to several times that obtained by the conventional method of increasing the angle of attack. A summary of circulation-control research is presented by Wood and Nielsen (1985).

A circulation-control wing test was recently completed in the Ames 6- by 6-Foot Transonic Wind Tunnel. The test was conducted to support the research needs of the NASA RSRA/X-Wing stopped-rotor research vehicle, which is a circulation-control rotor that can be stopped in the X-wing position for high-speed cruise (Wood and Nielson, 1985). The model was an aspect-ratio-four semispan wing mounted on the side wall of the wind tunnel. The airfoil was a 20%-thick ellipse, modified with circular leading and trailing edges of 4% radius, and had a 25.4-cm constant chord. This generic configuration does not represent a specific shape from current vehicle design concepts, which are in a state of development. A full-span, tangential, rearward-blowing, circulation-control slot was incorporated ahead of the trailing edge on the upper surface. The wing was tested at Mach numbers from 0.3 to 0.75 at sweep angles of 0° and +45° with internal-to-external pressure ratios of 1.0 to 3.0. Lift and pitching-moment coefficients were obtained from measured pressure distributions at five span stations. Surface-flow patterns were obtained using the oil-streak flow-visualization method. Boundary-layer and wake surveys with three- and five-hole flow-direction probes were obtained over the wing and in the wake near the midsemispan with the wing swept back 45°.

This paper presents selected pressure distributions and photographs of oil-flow patterns from this test. Boundary-layer and wake measurements are presented in a companion paper by Spaid and Keener (1986).

TEST FACILILTY

The Ames 6- by 6-Foot Transonic/Supersonic Wing Tunnel was chosen because the allowable model size is suitable for boundary-layer research. The tunnel is a variable-pressure, continuous-flow facility. The nozzle leading to the test section is of the asymmetric, sliding-block type that permits a continuous variation in Mach number from 0.25 to 2.3. The test section has a slotted floor and ceiling with 6% porosity and provisions for boundary-layer removal. The turbulence-velocity level is high, measured to be about 1.5% of the free-stream velocity.

MODEL

The model was a semispan wing incorporating circulation control by tangential blowing from a spanwise slot located ahead of a rounded trailing edge. The model was mounted on the side wall of the tunnel on a turntable that could be manually rotated through a -5° to +5° angle of attack range. The wing-root-mounting structure was covered with a fairing that had a 12.7-cm by 17.8-cm (5 × 7) elliptic transverse cross section. The cross section in the plane of symmetry had a length/major axis nose ratio of 1.0 and afterbody ratio of 1.5. Figure 1 is an artist's view of the model in the tunnel showing the effect of the jet flow from the slot on the airflow around the model. Figure 2 shows the model installation in the tunnel at both the 0° and 45° sweep positions. The resulting aspect ratios were 4.0 and 1.85, respectively, based on the normal component of the exposed span. Figure 3 shows three views of the model installation in the 0° and 45° sweep positions and a close-up view of the trailing-edge slot.

The wing section was designed with a simple 20%-thick elliptic airfoil, modified with circular leading and trailing edges of 4% radius, and had a 25.4-cm constant chord (fig. 4). This airfoil was similar to several previously tested circulation-control airfoils and was purposely selected to be generic and not to represent a specific shape from current vehicle design concepts. These concepts are in a state of development and it was felt that a generic shape would adequately serve the purpose of this test to explore the effect of sweep angle. A full-span, tangential, rearward-blowing, circulation-control slot was incorporated ahead of the trailing edge on the upper surface.

Design suggestions based on previous circulation-control tests were contributed by N. Wood of the Joint Institute for Aeronautics and Aeroacoustics of Stanford University and by E. Rogers and J. Abramson of the David W. Taylor Naval Ship Research and Development Center. Publications from their research are given in the summary paper of Wood and Nielsen (1985). The wing section follows closely the design concepts of Wood and Conlon (1983) and Wood and Sanderfer (1986). The model was designed in four parts (fig. 4), split along the plane of symmetry. The center of the model contained an internal plenum, which was connected to the external air supply at the wing root through the side wall of the tunnel. Ahead of the plenum

was a separate compartment to pass the pressure tubes from the forward parts to the wing root. The compartment was sealed from the plenum pressure with an O-ring seal. Such O-ring seals were also used between the forward parts and the slot and trailing-edge pieces, installed in a horizontal step so that a positive seal occurred when the top and bottom halves were bolted together. Several vertical posts, spaced every 7.11 cm spanwise, separated the split halves.

Figure 5 is a cross-sectional sketch showing the design of the slot and trailing edge. A leading and trailing radius of 4% was selected. From previous experience a nominal slot height of 0.0020 chord was recommended with a trailing-edge thickness of 0.0008 chord. For this particular model, the generating circle for the trailing edge was "rolled" forward along the lower surface of the generating ellipse until an acceptable gap occurred with the upper surface, forming the slot. The final design gap was $h = 0.483$ mm (REFERENCE $H/C = 0.0019$). The sharp slot trailing edge was removed to a trailing-edge thickness of $t = 0.0203$ mm (REFERENCE $t/c = 0.0008$), which is more controllable dimension than a sharp edge. The slot lip was designed with a 7° internal angle to the trailing-edge radius, forming a converging nozzle. This 7° internal angle was felt, from experience, to be the minumum angle required to avoid jet detachment from the Coanda surface. The remainder of the slot lower surface was faired forward with large radii, as shown. To allow adjustment of the slot height from the nominal design height, a flexure cutout was designed (as shown in fig. 4) with the objective that the radius be large enough that the outer surface would not experience a discontinuity in local slope and small enough that the cutout would not distort the shape from the internal pressure. The internal design of the trailing edge was finalized with a straight ramp to avoid a curvature that might induce Gortler vortices that would be fed into the jet. Such vortices have been observed in previous tests. Surface-pressure tubes in the slot piece were routed to the wing root through the flexure space, held in place with spot-welded metal strips and covered with a flexible epoxy. Surface-pressure tubes in the trailing-edge piece were routed through a slot cut into the inside surface and filled with epoxy.

Adjustment of slot height was provided by adjusting screws at several span stations. Fixing slot height was provided by setscrews placed ahead of each adjusting screw. This arrangement was determined from experience to be best for avoiding interaction of the two screws with the slot height, which would require several iterative adjustments. The two screws were placed in line (chordwise) with each other and with the support posts to reduce flow interference. A careful stress analysis was made of the flexure cutout and the effect of the adjusting screws.

From previous experience it was felt that several of the dimensions required close tolerances. The most critical tolerances were found to be the chordwise position of the slot lip with respect to the trailing edge and the trailing-edge contour. Thus, the trailing edge was chosen as a reference, with a tolerance of 0.050 mm for the slot-lip position and the trailing-edge radius along the length of the span. Machined vertical faces between the plenum and the rear pieces provided the necessary control of the tolerances between the rear and forward pieces.

For strength, corrosion resistance, and surface durability, the model was constructed from stainless steel and designed to withstand internal pressures of 60 psig.

The air supply was provided from the tunnel 80-psi dry-air sphere. The airflow was controlled by a regulator to set the total pressure in the wing plenum. An orifice plate in the system provided mass-flow measurements.

INSTRUMENTATION AND ACCURACY

The pressure instrumentation consisted of 252 orifices on the wing, installed at five spanwise stations (rows 1 to 5: $2y/b = 0.1$, 0.3, 0.5, 0.7, and 0.9, based on the exposed span at 0° sweep) and one row of orifices at the midspan of the wing-root fairing (fig. 6). More orifices were placed at row 4, $2y/b = 0.7$, especially over the trailing edge, to obtain more detail at one row. Additional orifices were placed at row 6 at a 45° angle between rows 3 and 4 ($2y/b = 0.5$ and 0.7) to assist in the analysis of the pressures at a sweep angle of 45° and to provide a row of orifices for boundary-layer measurements at this angle. Orifices were 0.50 mm in diameter, which is the standard wind-tunnel measurement, to avoid hole interference with the pressures. A 1.0-mm-diam tube was epoxied into a hole drilled into the back side of the orifice location. The tubes were routed to the wing root and through the side-wall turntable, as described in the MODEL section. Four pitot-static pressures and two thermocouples were installed internally. An accelerometer was installed in the wing tip to measure the frequency and amplitude of the vibrations of the steel wing, which was designed to be rigid.

The surface static pressures were measured using electronically actuated pressure-scanning valves containing pressure transducers that were connected to an automatic data-recording system. The self-calibrating feature of the scanning valves provided an accuracy of about 0.25% full scale of the ±8.62 N/sq cm (±12.5 psi) transducers, between ±0.006 and ±0.01 in pressure coefficient at the higher speeds. Tunnel test conditions were measured with precision pressure recorders giving a Mach number accuracy of about ±0.002. Tunnel-static pressure was measured on the tunnel wall 10 wing-chord lengths ahead of the wing-root leading edge. The angle of attack was set manually by rotating the wall turntable and setting the angle with an inclinometer with an accuracy of ±0.03°.

SIMPLE-SWEEP THEORY

In a selecting the test conditions for the two sweep angles, it was desired to test the application of simple-sweep theory to the pressure distributions. The theory applies to a wing section of an infinite or very-high-aspect wing. Therefore, it was realized that the present wing could have both wing-tip and wing-root

fairing effects. Nevertheless, it was of interest to analyze the midspan pressures in light of the simple-sweep theory.

The physical concept of the simple-sweep theory can be described as follows: suppose that a very long wing of constant chord and constant airfoil section is mounted at right angles in a wind tunnel through slots in the side wall. If the wing is drawn through the slots at constant speed, w, it is reasonable to believe that the pressures over the wing will not change (in the first order) from what they were when the wing was stationary. The resultant free-stream velocity, V, relative to a given point on the wing will then act at the angle, $\sin^{-1}(w/V)$, to a plane perpendicular to the wing leading edge, in which lies the normal wing chord and the normal velocity, VN, of the tunnel. Hence, the wing pressures are independent of w and dependent only on the projection of the relative free-stream velocity upon a plane perpendicular to the wing leading edge (the normal plane). Therefore, if a swept wing is tested at Mach number, M_∞, sweep angle, Λ, and angle of attack, α, the following expressions relate the aerodynamic pressure distributions, loading, and moments to the equivalent values at the normal Mach number, M_N:

Swept pressure distribution = Equivalent unswept pressure distribution
(at equivalent Mach number)
for this test, $\Lambda = 45°$

Mach number:
equivalent Mach number = $M_N = M_\infty \cos^2\Lambda = 0.7\ M_\infty$

Pressure Coefficient
Pressure, (swept section) = Pressure, (normal section)
$C_p = (p - p_\infty)/q_\infty$; $C_{p,n} = (p - p_\infty)/q_n$
$q_\infty = q_n/(\cos^2\Lambda)$

therefore,
$C_\ell = C_{\ell,n}\ (\cos^2\Lambda) = 0.50\ C_{\ell,n}$

Lift and Moment Coefficients:
load (swept) = load (normal)
$c_p = c_{p,N}\ (\cos^2\Lambda) = 0.50\ c_{p,N}$
c_m (sweep) = $c_{m,N}\ (\cos^2\Lambda)$ at $x = c/2$

Mass-Flow Coefficient:
jet velocity for swept wing, $V_j = V_{j,N}$ since jet velocity is normal to trailing edge

mass flow (swept) = mass flow (normal)

therefore,
$C_\mu = C_{\mu,N}\ (\cos^2\Lambda) = 0.50\ C_{\mu,N}$

Reynolds number:

$R_{e,N} = R_e, (\cos^2\Lambda)$ has no theoretical influence in the simple theory. The boundary-layer flow must be similar (no change in state that affects the pressure distribution). This occurs only for a laminar boundary layer. Allowing a turbulent boundary layer by keeping the location of transition common to both the swept wing and the equivalent unswept wing is not sufficient since the turbulent boundary layer does not scale the same in the spanwise direction as in the chordwise direction, as a laminar boundary layer does.

Angle of attack:

α (swept) = α (normal)/$(\cos^2\Lambda)$

Note: Finite span generates an induced angle of attack, in addition to the geometric angle generated by sweep. Also, if the aspect ratio is small, there can be root effects, like the effect of the fairing for this wing.

TEST CONDITIONS AND PROCEDURES

Jet-blowing effectiveness was first evaluated with tunnel air off. Wing pressures were then measured without boundary-layer trips at M = 0.70 at 0° sweep angle. Sublimation flow-visualization tests showed that boundary-layer transition occurred near the midsection. Boundary-layer trips were then installed on the wing at 0.09 chord using sifted glass spherules having a nominal size of 0.23 cm, selected from standard curves. Sublimation flow-visualization tests made at a Mach number of 0.70 verified that this size was adequate at both the 0° and 45° sweep angle to cause transition at the trips.

Pressures were measured over the wing and wing-root fairing at Mach numbers of 0.3, 0.4, and 0.5 at 0° sweep angle and at Mach numbers of 0.425, 0.566 and 0.7 (determined from simple-sweep theory, M/cos 45°) at 45° sweep angle. Angles of attack were 0°, ±2.5°, and ±5° at 0° and 45° sweep angles and ±1.8°, and ±3.5° additional angles at 45° sweep (determined from simple-sweep theory, α cos 45°). Reynolds number was limited to a maximum of 3 million (based on wing chord) to keep the wing loads within the design conditions. Most of the tests were conducted at a total pressure of 1 atm.

Oil-flow-visualization tests were made at both sweep angles at several Mach numbers. It was found that for most cases a single spanwise strip of oil on each surface behind the boundary-layer trips and a sheet of oil on the wingtip produced adequate results.

DISCUSSION

Tunnel Wind-Off Tests

An initial evaluation of the performance of the Coanda surface can be determined with jet-blowing tests alone. This test would follow the model inspections of the Coanda surface as described by Wood and Conlon (1983). Accordingly, a tunnel wind-off test was made with a blowing-pressure ratio of 1.8. The jet flow formed a long "tuft" which followed the trailing edge and blew forward along the lower surface. The flow even tried to turn around the leading edge but finally separated. This test showed that the Coanda surface was working effectively. The tuft was traversed along the span and showed a discontinuity in the flow along the lower surface at about one-third span. Inboard, the tuft was inclined toward the root at a noticeable angle. According to previous experience the change in flow angle over the lower surface results from internal flow disturbances that are amplified in the flow over the Coanda surface. For the present model it was concluded that the the flow disturbance resulted from the design of the air supply at 0° sweep angle through the forward air port, which directed airflow toward the trailing edge at about one-third span (fig. 6). At 45° sweep, this disturbance did not occur since the air was supplied through the rearward air port, which was directed spanwise.

Next, a pitot-pressure survey was made along the span of the jet. The pitot pressure was uniform along the span at both sweep angles, indicating that the internal flow disturbances at 0° sweep were not severe. No recognizable problems were caused by this internal flow disturbance during the tests with the tunnel wind on.

Oil-Flow Visualization

Selected oil-flow-visualization photographs are shown for a sweep angle of 45°. Figure 7 is a photograph of an oil-flow test on the upper surface at a sweep angle of 45°, $M_\infty = 0.425$, $\alpha = 0°$, and no jet blowing. The boundary-layer trip strip can be seen at 0.095 chord, as can the chordwise and spanwise strips of transparent tape protecting the orifices. Oil was applied behind the trips at about 0.20 chord. The boundary layer separates ahead of the jet slot (located at 0.96 chord) as determined by the oil streaks turning outboard to run spanwise, forming an oil-flow separation line.

The next series of oil-flow photographs (fig. 8) are for the same test conditions ($M_\infty = 0.425$, $\alpha = 0°$) but with jet blowing at a pressure ratio of 1.8. The top-surface flow (fig. 8(a)) is almost streamwise over the swept wing. (The separated flow near the slot with no blowing attaches quickly with small blowing.) Near the slot the flow turns slightly inboard toward the jet flow, which is nearly normal to the trailing edge. There is no prominent disturbance of the surface flow at either end of the slot. It is impressive that at the wing root the jet is detached on the fairing but strongly attaches to the Coanda surface within about 1.5 cm of the fairing. The inboard edge of the jet sheet must roll up into a vortex as evidenced by the print of the trailing vortex on the fairing after tunnel

shutdown. The wingtip flow is strongly entrained into the jet flow. Close post-run inspections of the oil flow at the outboard end of the slot revealed a trace of the onset of the trailing vortex that forms at the outboard edge of the jet sheet, as depicted in figure 1. The lower-surface view (fig. 8(b)) shows the location of the lower-surface flow separation caused by the Coanda separation. The oil streaks turn outboard forming an oil-flow separation line. At this blowing-pressure ratio of 1.8, which is before jet stall, the separated lower-surface and upper-surface flows come together in the downwash very close to the trailing edge, enclosing the separated region into a bubble-like flow (see interferograms and shadowgraphs in Wood and Nielsen, 1985).

The wingtip flow is seen in the top and bottom views from the left-side tunnel window (figs. 8(b) and (c)). The top- and bottom-surface flow is directed toward the tip. Therefore, the flow around the tip is similar to the flow on the lee side of an ellipsoid. Around the leading edge, the flow separates in a laminar separation line that extends back to the boundary-layer trips. Behind the trips the boundary-layer flow is turbulent so that the flow separates at a turbulent separation line that is located farther around the lee of the tip (most clear in fig. 8(c)). (For a circular body the laminar and turbulent separation lines are located about 90° and 140°, respectively, from the the windward crossflow stagnation line.) To the lee of the primary separation lines are the secondary separation lines. The tip-flow pattern is obviously asymmetric, so that this flow must contribute two asymmetric vortices to the tip flow field, in addition to the vortex at the outboard edge of the jet sheet starting at the end of the slot. The asymmetry of the tip vortices is probably affected by a change in angle of attack.

Figures 9 and 10 show oil-flow photographs for the case of $\alpha = 5°$ and $M_\infty = 0.425$ and 0.70. At this angle of attack it is more difficult for the jet to maintain attached flow on the upper surface. Fluorescent oil was injected through selected orifices. Instead of forming a narrow streak the oil spreads slightly. Figure 9 shows three views of the flow without blowing and with blowing pressure ratios of 1.2 and 1.3. At blowing pressure ratios up to 1.2, the flow separates ahead of the jet slot as indicated by the oil streaks turning outboard, but at a blowing pressure ratio of 1.3 the flow attaches because of the influence of the jet. The photographs also show that a leading-edge separation bubble exists at about 0.04 chord. The oil streak from the leading-edge orifice feeds oil into the bubble so that the oil flows spanwise in the bubble to the wing tip. If a similar oil streak is injected near the wing root, the full spanwise extent of the bubble would be revealed. This bubble is not revealed by smearing a film of oil at several places along the leading edge, although in other tests similar bubbles have been revealed by this method. The bubble exists at all pressure ratios tested. It is interesting that the bubble is located close to the point of tangency between the circular leading edge and the ellipse. Figure 10 shows that at $M_\infty = 0.70$ even a high blowing pressure ratio of 2.0 is not sufficient to induce the flow to attach.

Pressure Distributions

The measured pressure distributions were analyzed using the simple-sweep theory. Figure 11 illustrates the collapse of the section lift data for the swept and unswept configurations at the 70% spanwise location. Data for the swept configuration have been corrected using the standard equations to account for sweep on the angle of attack and dynamic pressure as previously stated. The correction to the dynamic pressure has also been introduced into the blowing momentum coefficient. It is clear that overall performance trends are repeated quite accurately, including jet-stall and α stall locations. The slight variations in the unblown lift curve slope were isolated to an effect of changing the location of the model in the wind tunnel working section for the two configurations. A large, static-pressure gradient was found to exist in the working section and was observed by a vertical shift of the presesure-coefficient distributions in the swept configuration. This is indicative of a change in the local static pressure at the measurement station.

The agreement between the swept and the unswept configurations was observed at each of the Mach number combinations that were tested. However, analysis of all the data shows that increases in the maximum lift coefficient were obtained at the highest Mach number (0.5 normal to the leading edge), the cause of which has not yet been isolated but is the subject of ongoing investigations.

Figure 12 illustrates the difference between the two configurations in terms of spanwise load distribution. For the unswept case, the wing is fairly uniformly loaded with a tip lift loss initiated at approximately 0.70 span (1 chord). For the swept configuration, an asymmetric loading is observed as is typical for a conventional swept wing. This asymmetry is a result of the changes in the downwash distribution caused by curvature of the bound vortices at the tip and root of the wing. Further analysis has recently shown that the downwash at the 0.70 spanwise station was identical for both the swept and unswept configurations, enabling the direct comparison of the section characteristics, as in figure 13. Also shown in figure 12 are the points at which jet stall was first observed (indicated by the dotted lines). While it is seen that the tip stalls first in the swept configuration for this set of conditions, this was not verified as a typical performance trend. it was observed, however, that jet stall appeared at the points of maximum downwash, which could be at any point on the span.

Figure 13 shows that the data are not significantly affected by the free-stream Mach number. The initial lift augmentation is defined as the slope of the lift coefficient vs. blowing momentum curve. The agreement is quite satisfactory for both the 0.70 (row 4) and 0.90 (row 5) spanwise stations. These data were taken at a fixed geometric angle of attack and the levels of lift augmentation are in good agreement with previous two-dimensional data.

A principal difference between swept and unswept wings is the induced downwash distribution. Recently, it has been shown that the induced angle of attack of a circulation-control airfoil may be deduced from examination of the variation of the mid-chord pitching moment with lift coefficient (Wood and Rogers, 1986). For a two-dimensional airfoil, the mid-chord pitching moment is decoupled from the lift as a

result of blowing and becomes a function of only the angle of attack. Thus, in figure 14, the slopes of the lines represent a combination of a change in angle of attack caused by tunnel interference and a change resulting from the imposed downwash distribution. For the unswept configuration, a trend of increasing downwash toward the tip is evident, while the trend is clearly reversed for the swept configuration. Since the variation of the mid-chord pitching moment with angle of attack is known, the actual downwash angles may be deduced. Results are given in figure 15. The unswept results are compared with a simple analysis based on a series expansion representation of the spanwise load distribution. The agreement is satisfactory and provides some confidence in the extension of the empirical technique to the swept configuration. Results for the swept case show a rotation of the distributions in a clockwise sense which indicates increased downwash at the root and decreased downwash at the tip. This trend was observed for all test conditions. It is also interesting to note the similarity in the downwash levels at the 0.70 spanwise location; this qualifies the agreement between the section lift data shown in figure 11.

CONCLUSIONS

A preliminary wind-tunnel investigation of the aerodynamics of a circulation-control, semispan wing model at two sweep angles was conducted at Mach numbers ranging from 0.3 to 0.75, angles of attack from -5° to +5°, and internal-to-external pressure ratios of 1.0 to 3.0. Conclusions from the pressure distributions at 0° and 45° sweep and photographs of oil-flow patterns at 45° sweep show:

1. The oil-flow tests at 0° angle of attack with no blowing show that the boundary layer separates just ahead of the slot.

2. With jet blowing, the wing-surface flow is attached and nearly streamwise away from the leading edge at a 45° sweep. There is no prominent flow disturbance at each end of the slot. The wingtip flow is strongly entrained into the outer jet flow. The lower-surface boudnary layer separates ahead of the Coanda-surface separation.

3. The wingtip flow pattern is similar to that of the lee side of an ellipsoid at a 45° angle of attack. An asymmetric vortex-separation pattern occurs with primary and secondary separation lines.

4. At a 5° angle of attack it is more difficult to attach the separated flow ahead of the slot with jet blowing at the lower speeds. At Mach 0.7, the flow cannot be attached at any blowing-pressure ratio.

5. When conventional corrections are applied at the 45° sweep position, no additional corrections are necessary to account for changes in blowing efficiency.

6. An empirical technique for estimating the downwash distribution of a swept wing has been validated with the swept-wing data and could be used to investigate three-dimensional effects on a circulation-control wing.

RECOMMENDATIONS

Further experiments are necessary on generic configurations to fully validate the use of simple-sweep theory. Configurations with both increased aft sweep angles and forward sweep angles need to be investigated over a range of slot blowing.

REFERENCES

1. Spaid, Frank W.; and Keener, Earl R.: Boundary-Layer and Wake Measurements on a Swept, Circulation-Control Wing. Circulation Control Workshop, NASA Ames Research Center, Feb. 18-20, 1986. NASA CP-2432, 1986. (Paper 11 of this compilation.)

2. Wood, Norman J.; and Conlon, John A.: The Performance of a Circulation Control Airfoil at Transonic Speeds. AIAA Paper 84-0083, Jan. 1983.

3. Wood, N. J.; and Nielsen, Jack N.: Circulation Control Airfoils Past, Present, Future. AIAA Paper 85-0204, Jan. 1985.

4. Wood, N. J.; and Rogers, E. O.: An Estimation of the Wall Interference on a Two-Dimensional Circulation Control Airfoil. AIAA Paper 86-0738CP, March 1986.

5. Wood, Norman J.; and Sanderfer, Dwight T.: Transonic Performance of Two Circulation Control Airfoils. NASA TM X-86767, 1986.

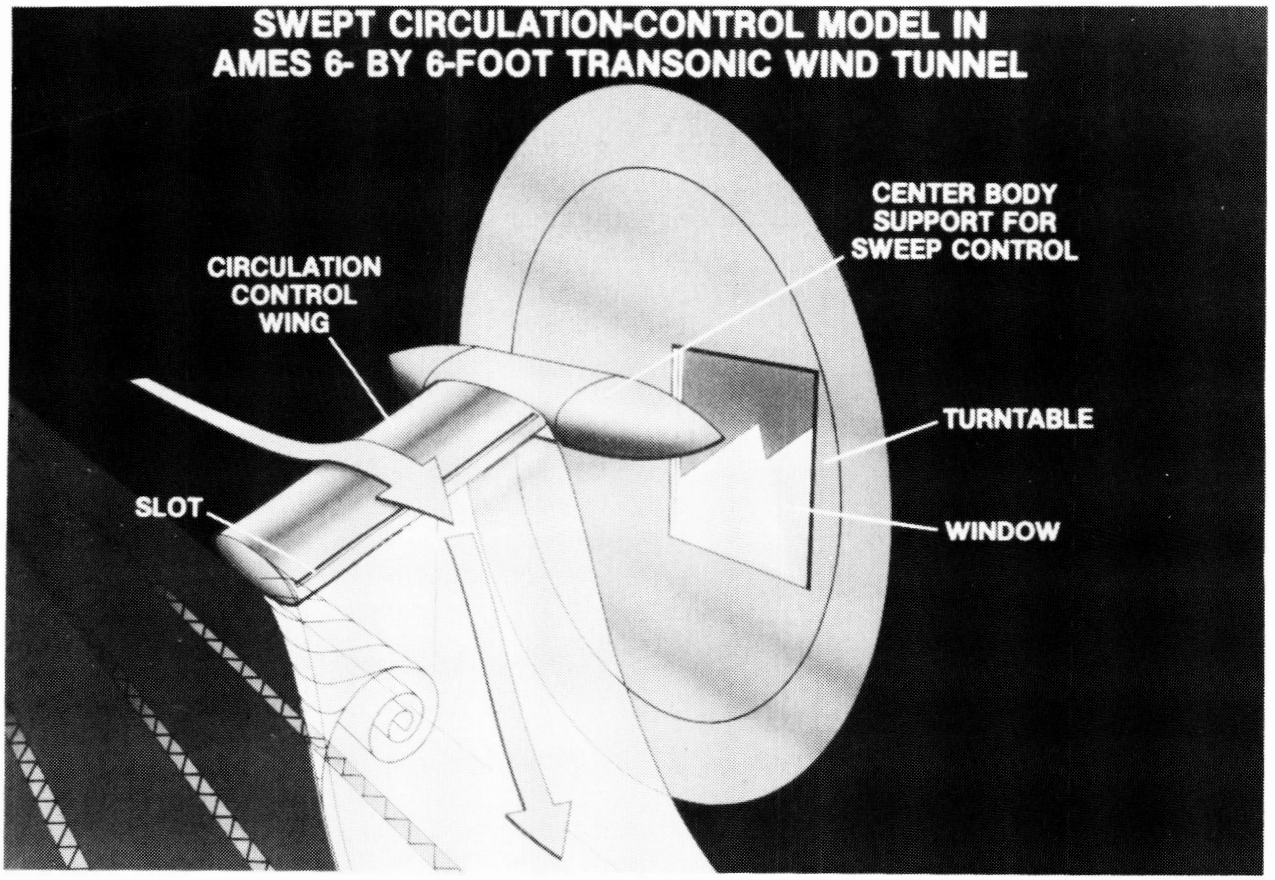

Figure 1.- Artist's view of model and flow field in Ames 6- by 6-Foot Transonic/Supersonic Wind Tunnel.

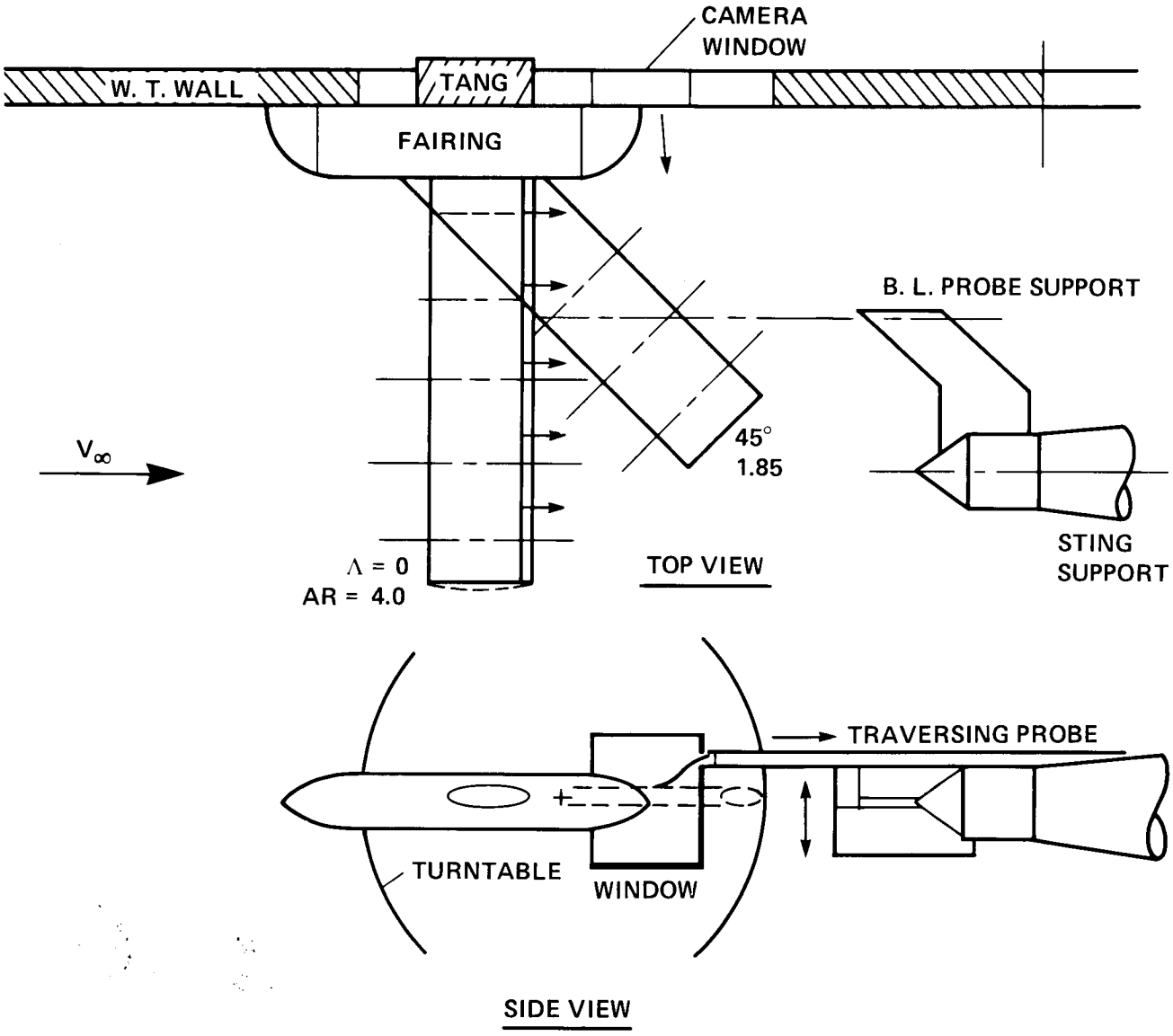

Figure 2.- Sketch of wing installation.

(a) 3/4 front view, sweep angle = 0°.

Figure 3.- Wing installation; sweep angle = 0°.

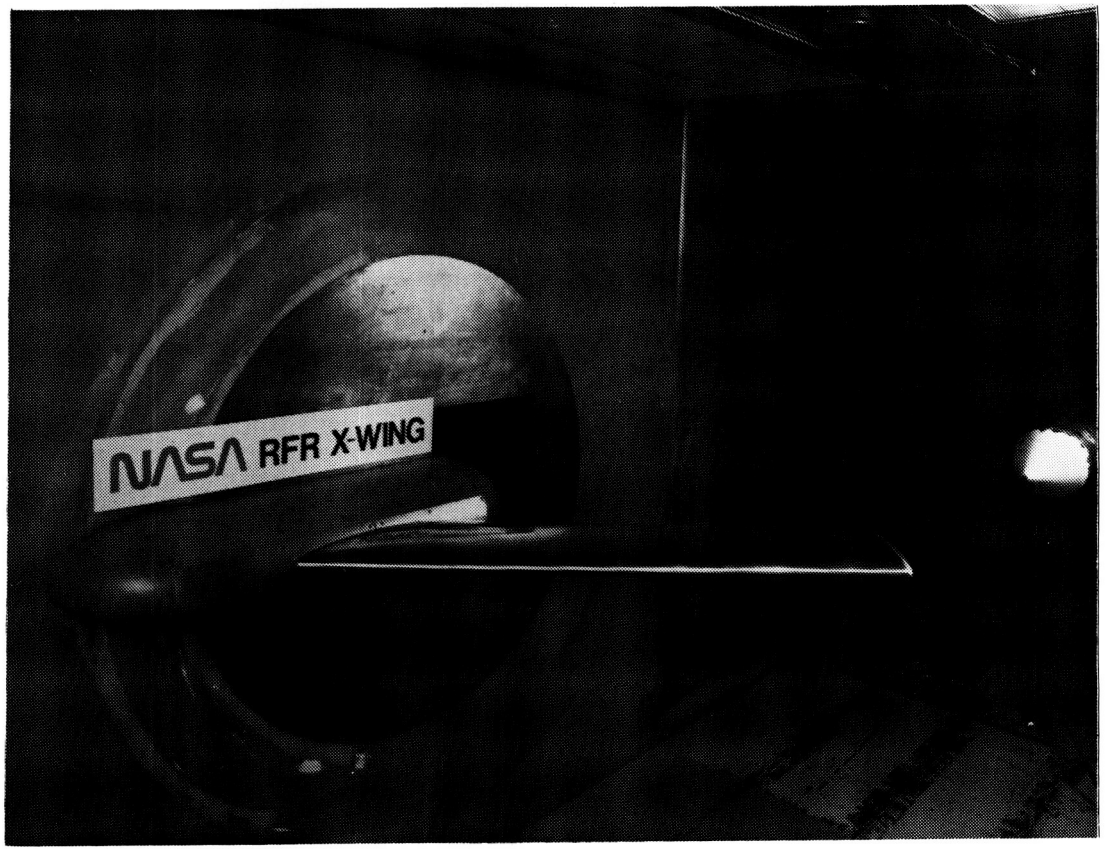

(b) 3/4 front view, sweep angle = 45°.

Figure 3.- Continued.

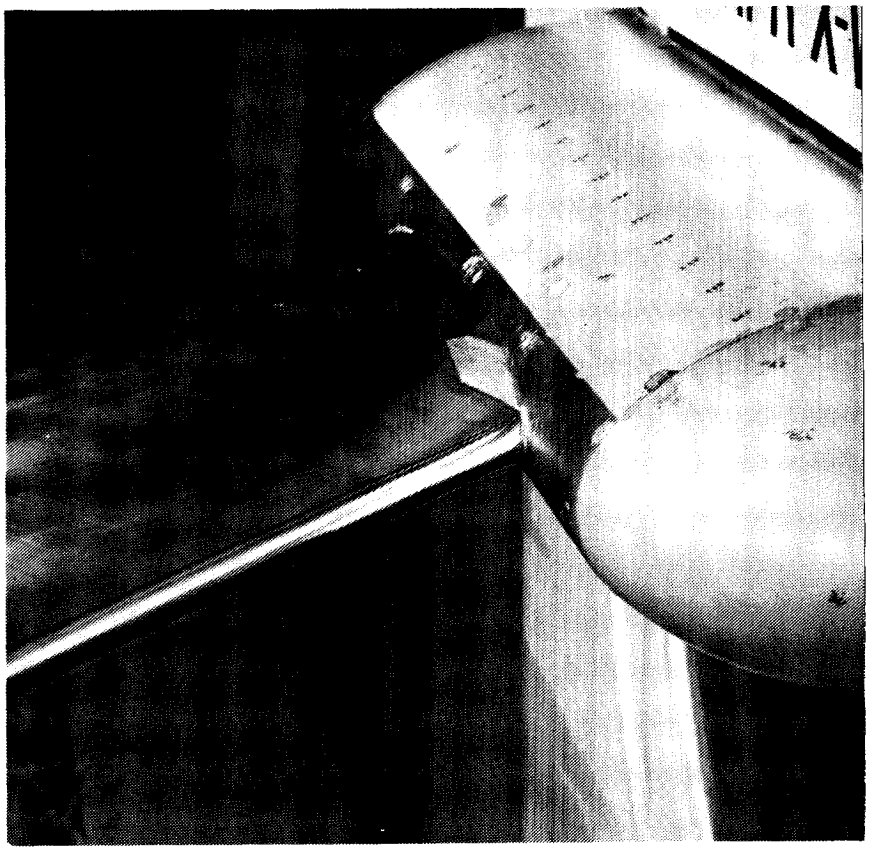

(c) Closeup-view of trailing-edge slot sweep angle = 45°.

Figure 3.- Concluded.

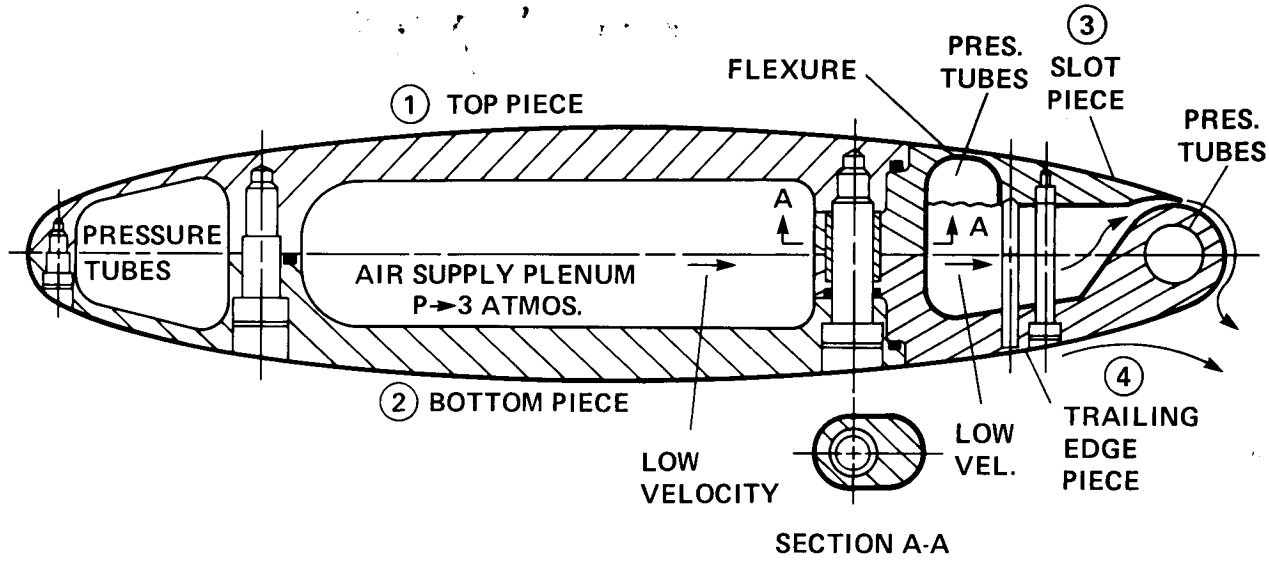

Figure 4.- Wing section showing four-piece construction, bolts setscrew, and adjusting screw for slot height.

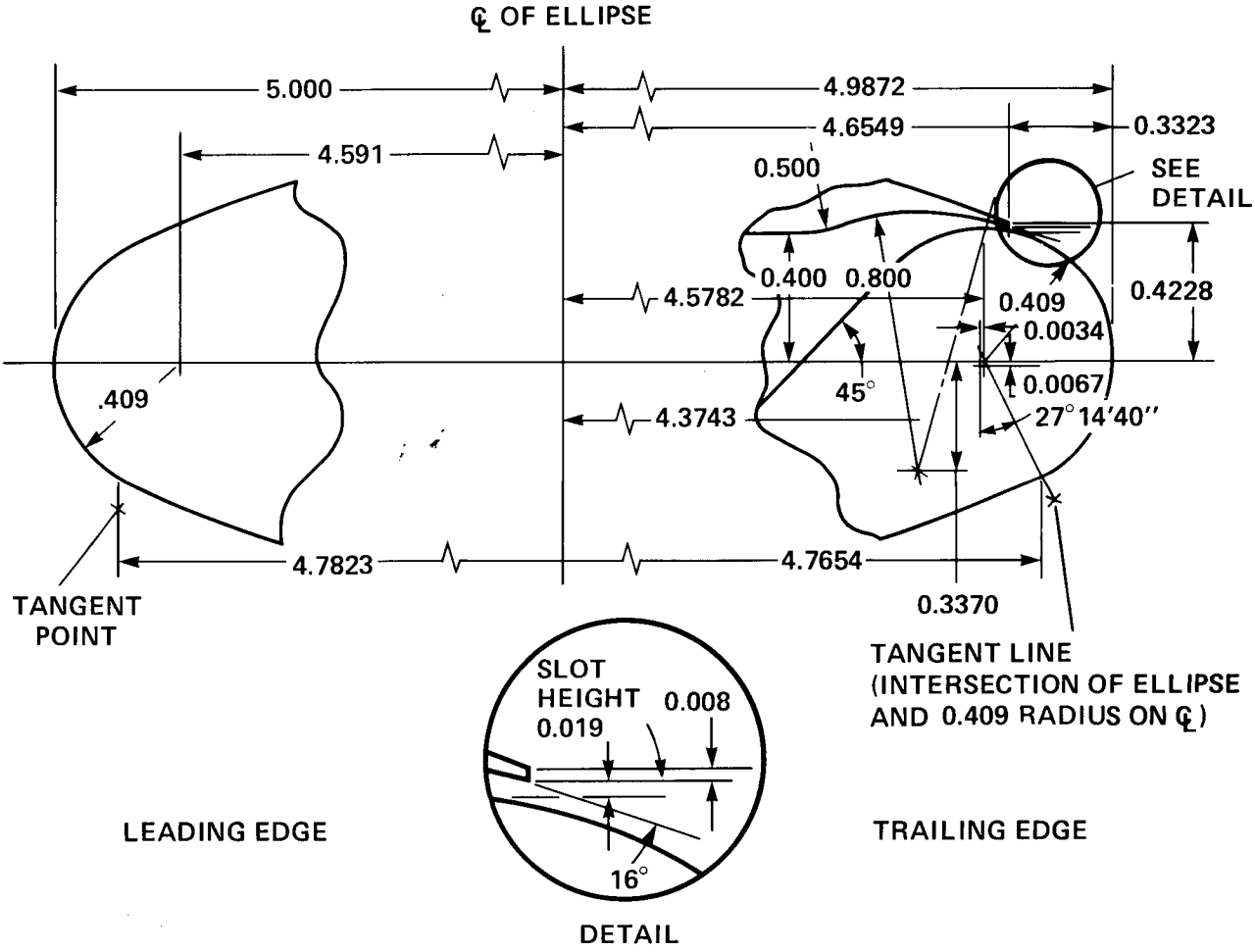

Figure 5.- Details of slot and trailing-edge design of the present model.

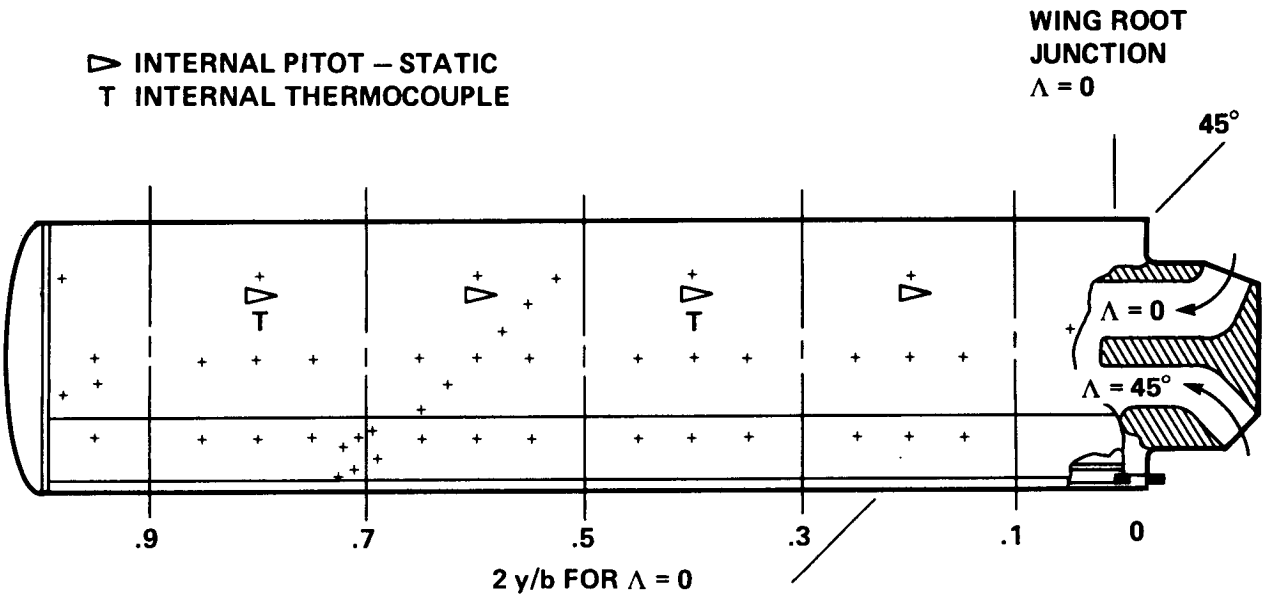

Figure 6.- Layout of static-pressure orifices on upper surface and air supply passage.

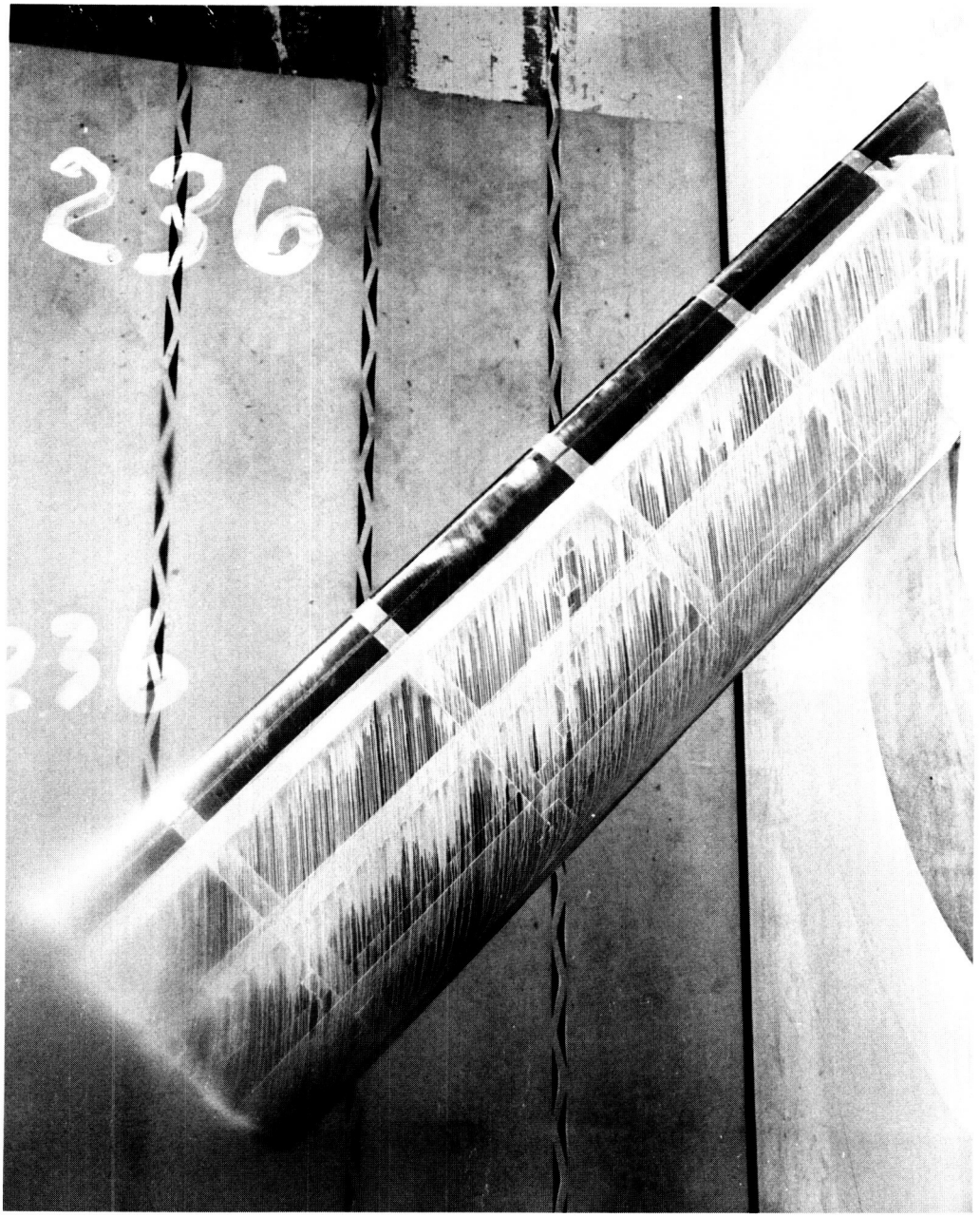

Figure 7.- Oil-flow photograph of upper-surface flow pattern with no jet blowing; $M = 0.425$, $\alpha = 0°$.

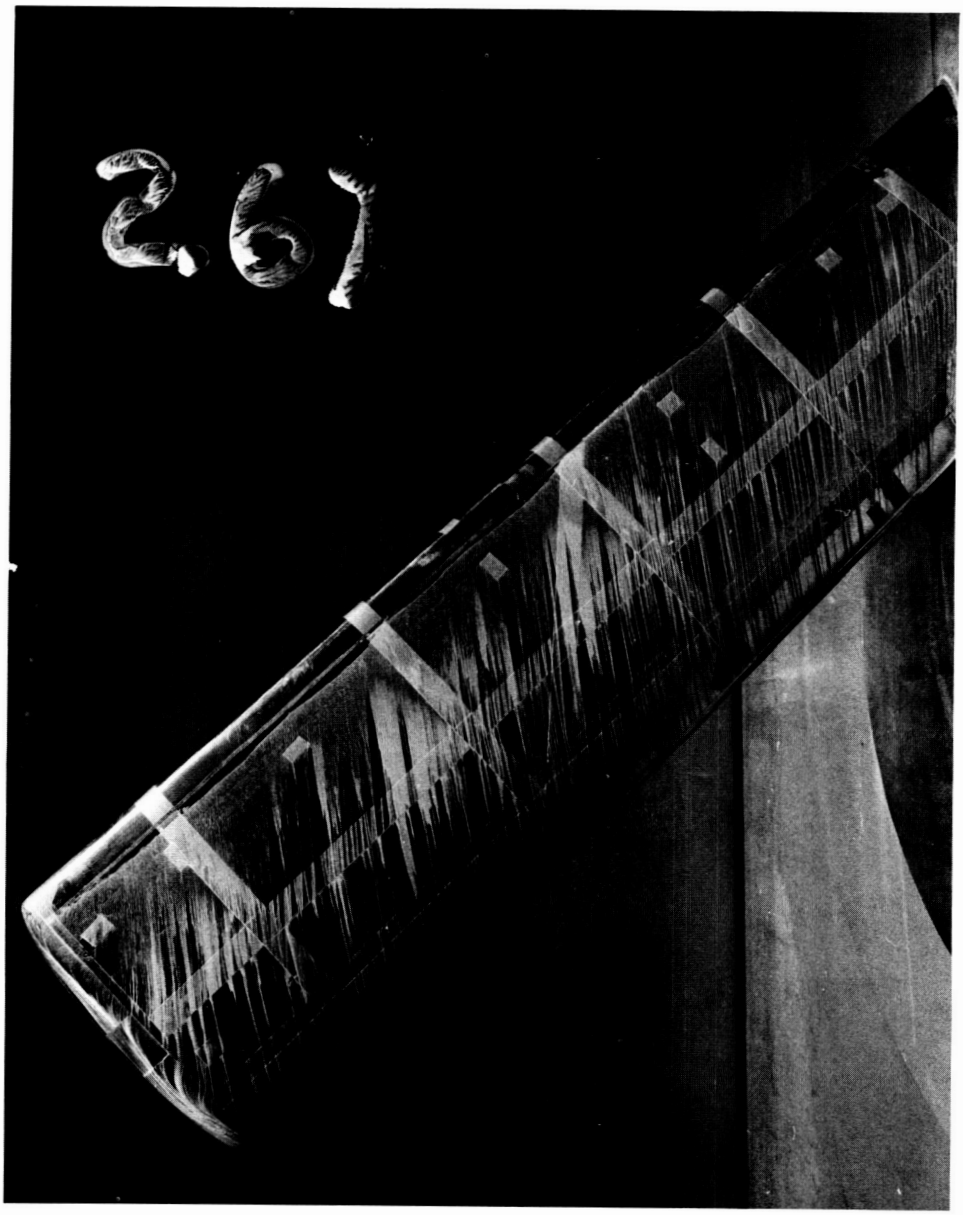

(a) Upper surface view.

Figure 8.- Oil-flow photographs of upper- and lower-surface flow patterns with jet blowing; M = 0.425, α = 0°, pressure ratio of 1.8.

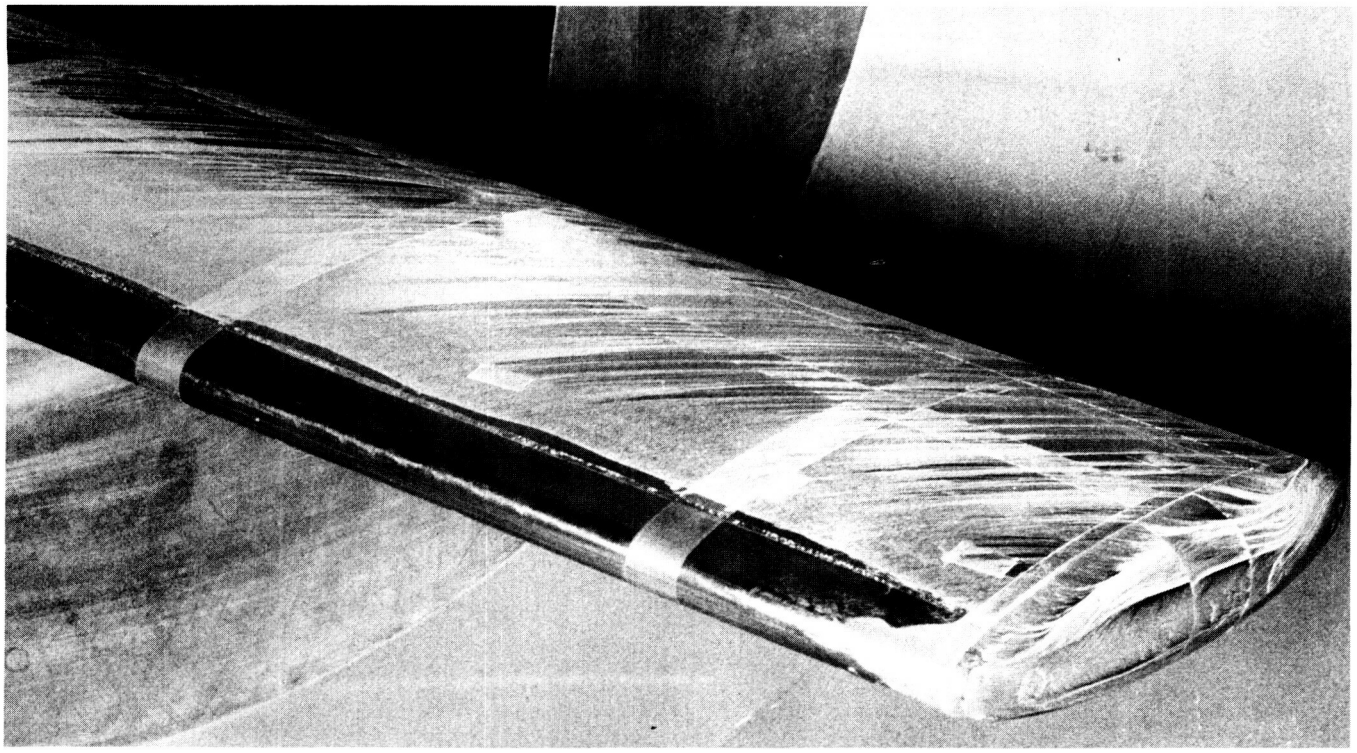

(b) Upper surface and end view.

(c) Lower surface and end view.

Figure 8.- Concluded.

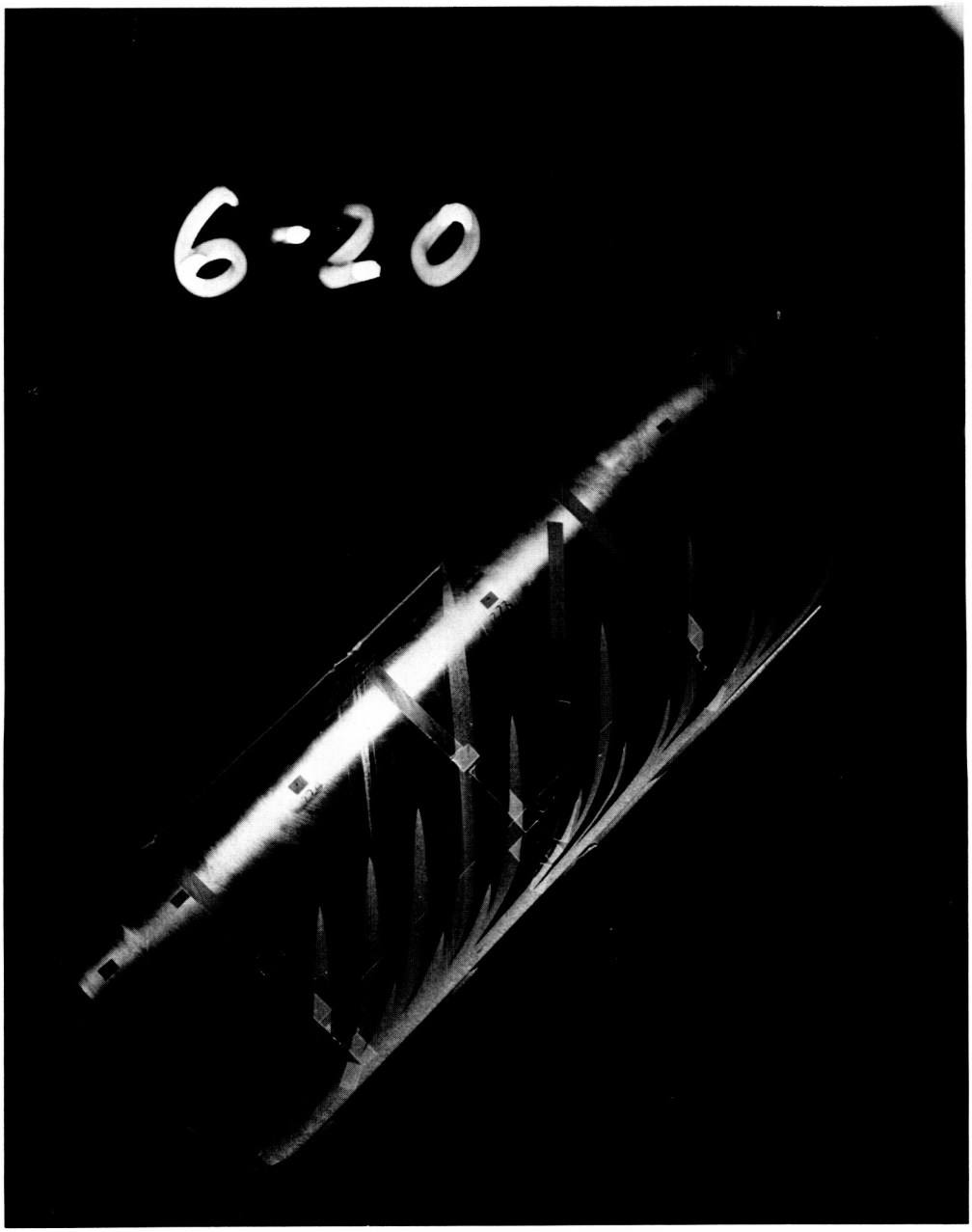

(a) pressure ratio of 1.0

Figure 9.- Oil-flow photographs of upper surface flow patterns at $\alpha = 5°$, $M = 0.425$.

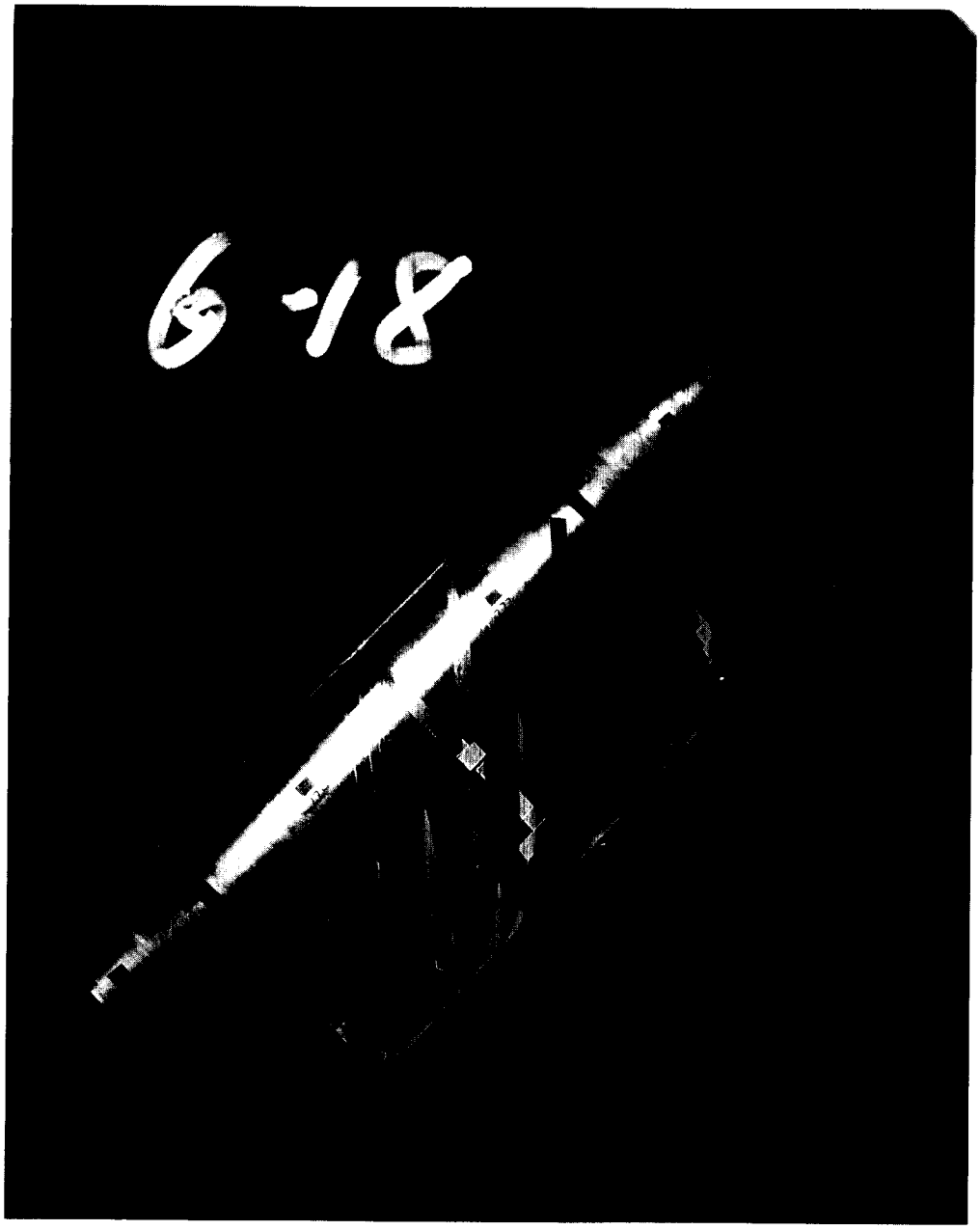

(b) pressure ratio of 1.2

Figure 9.- Continued.

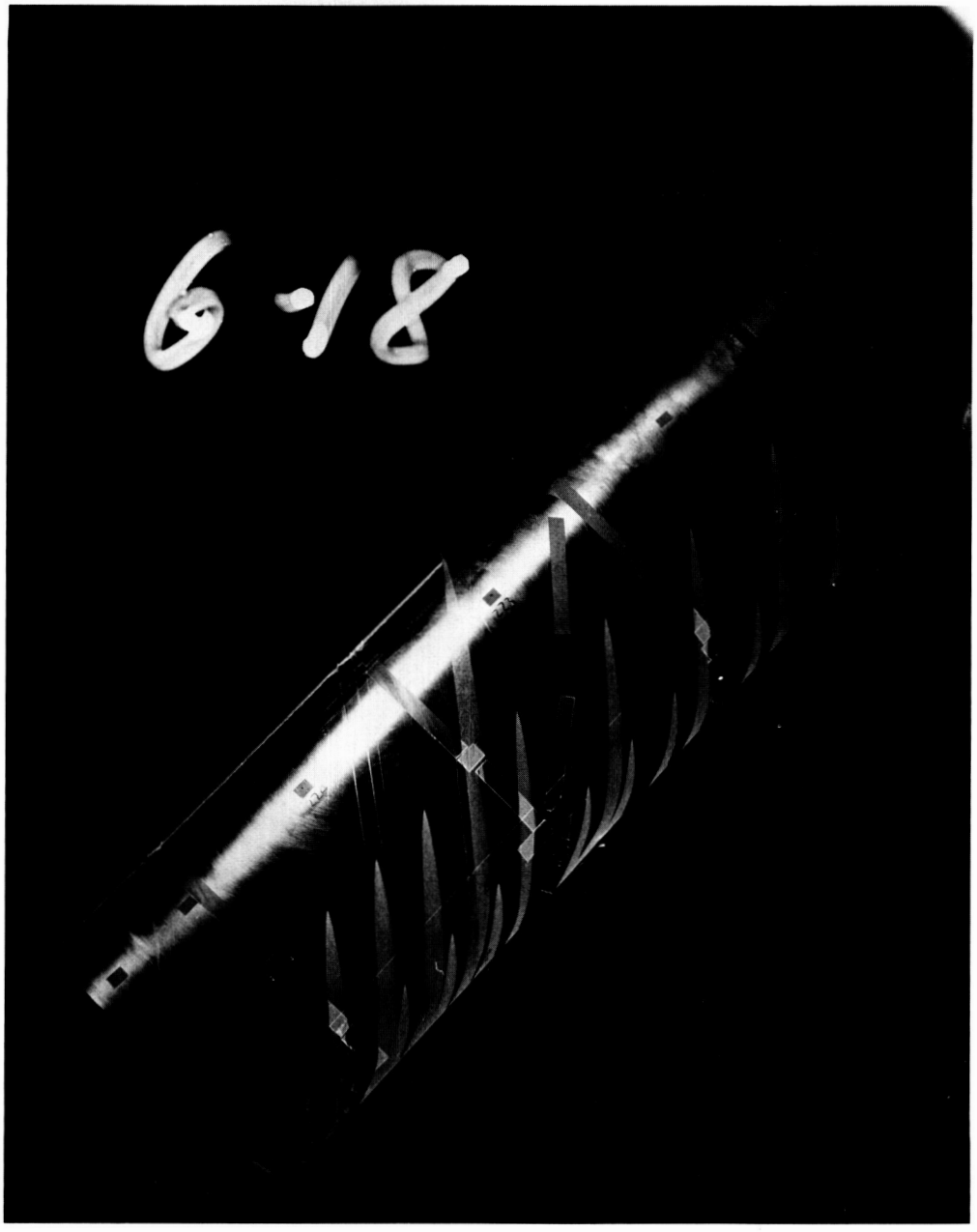

(b) pressure ratio of 1.2

Figure 9.- Continued.

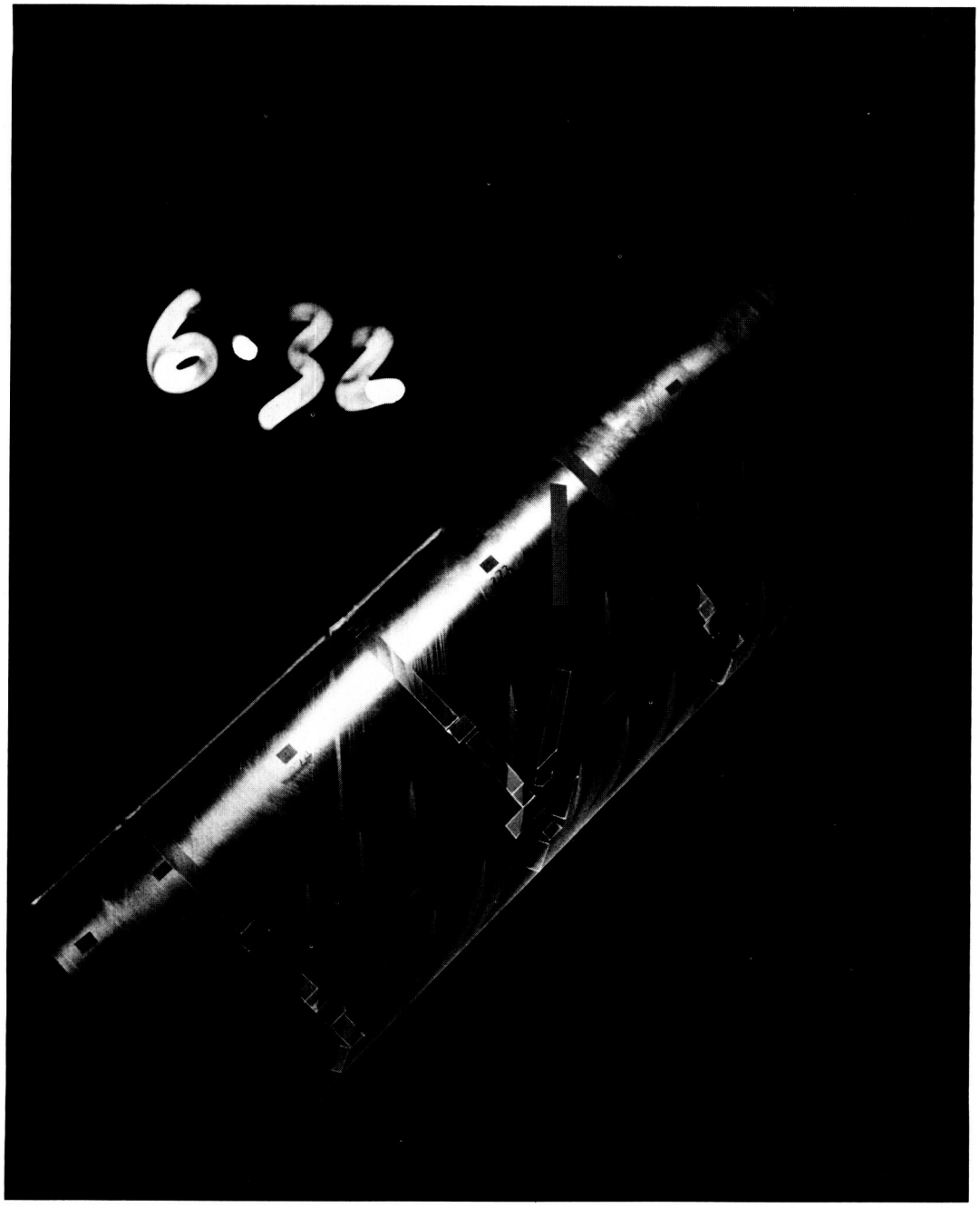

Figure 10.- Oil-flow photograph of upper-surface flow pattern at $\alpha = 5°$, $M = 0.70$, pressure ratio of 2.0.

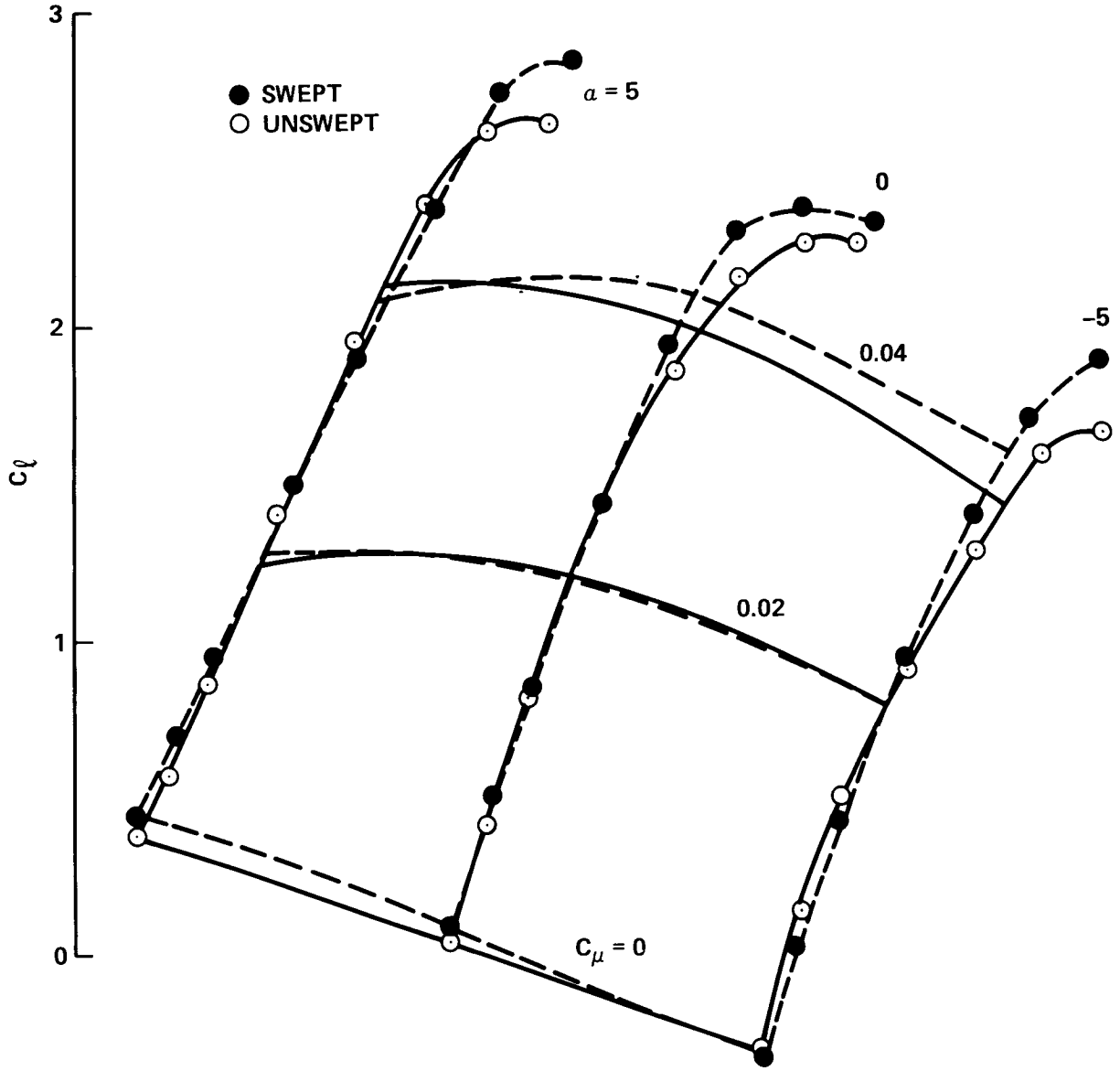

Figure 11.- Collapse of swept/unswept section-lift coefficient at M_∞ = 0.425 (swept)/M_∞ = 0.3 (unswept).

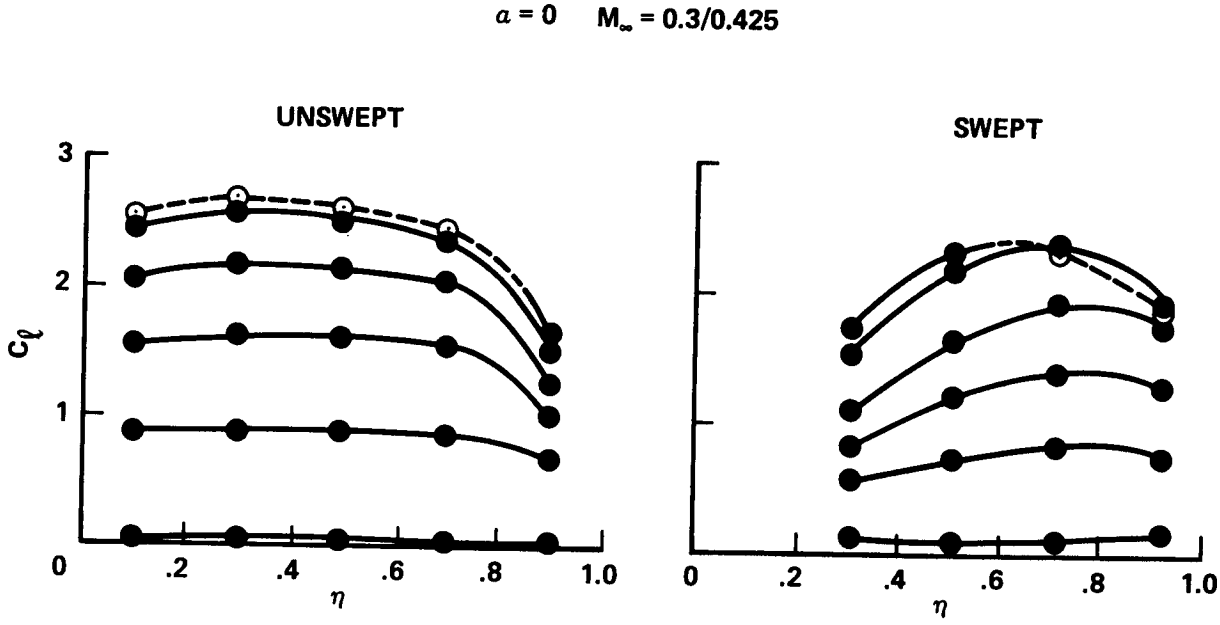

Figure 12.- A comparison of spanwise loading for swept/unswept configurations; $M_\infty = 0.425$ (swept)/$M_\infty = 0.3$ (unswept), $\alpha = 0°$.

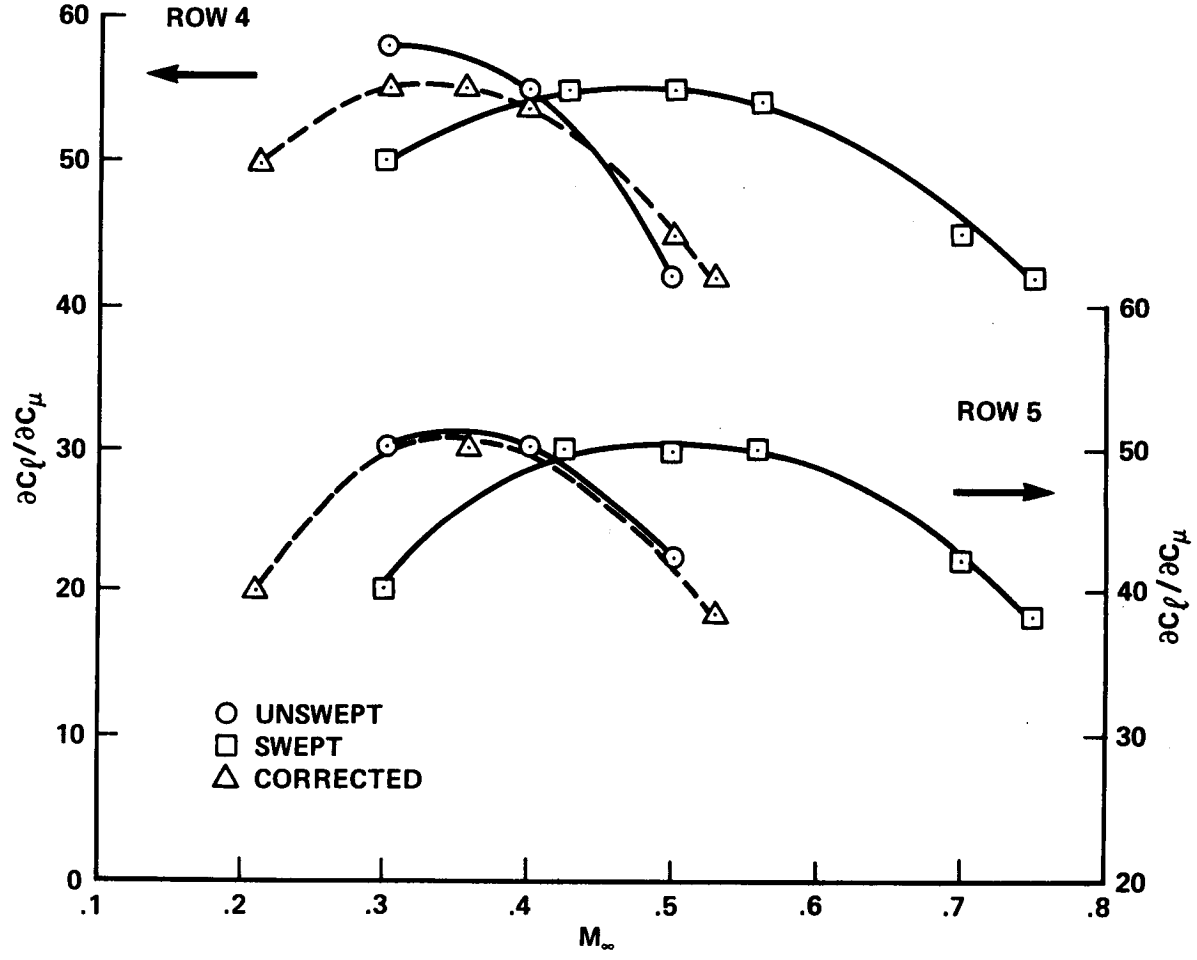

Figure 13.- A comparison of initial lift augmentations for swept/unswept configurations, $\alpha = 0°$.

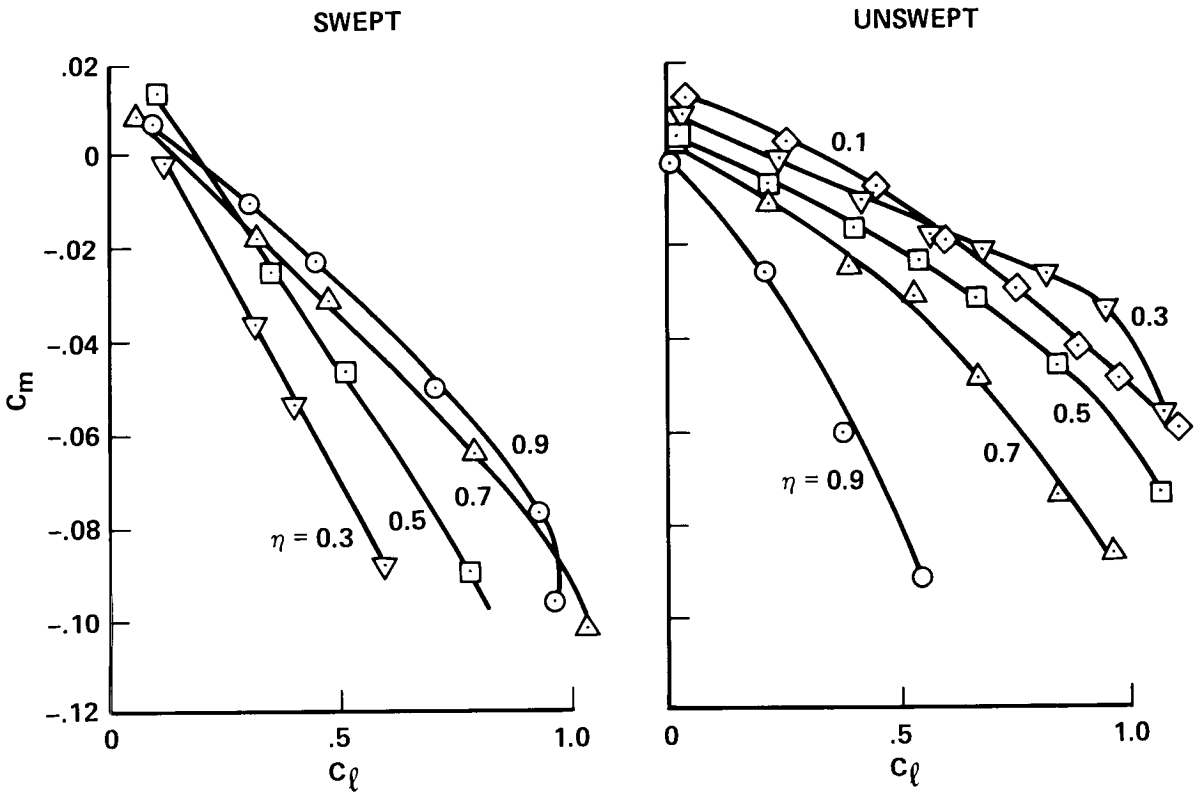

Figure 14.- Experimental results for the variation in mid-chord pitching moment with M_∞ = 0.425 (swept)/M_∞ = 0.3 (unswept), α = 0°.

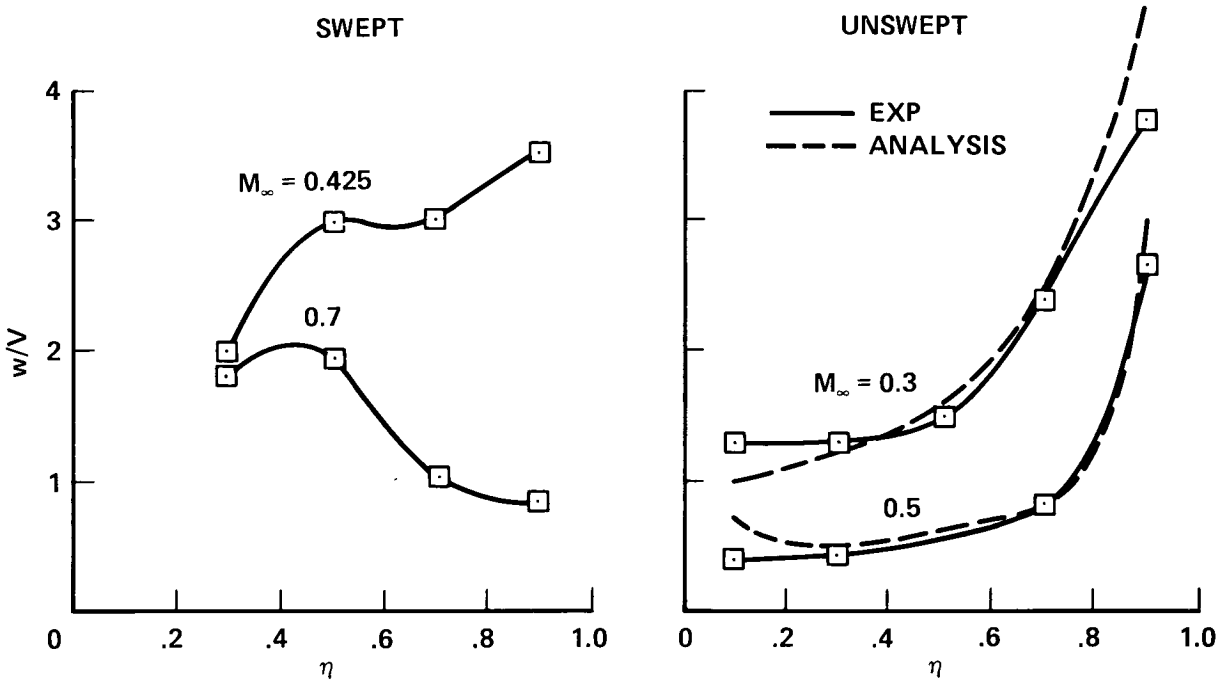

Figure 15.- Different downwash distributions for swept/unswept configurations, α = 0°.